STEM CELLS®

REGENERATIVE MEDICINE

Debrided Skin as a Source of Autologous Stem Cells for Wound Repair

SHANMUGASUNDARAM NATESAN, NICOLE L. WRICE, DAVID G. BAER, ROBERT J. CHRISTY

United States Army Institute of Surgical Research, Fort Sam Houston, Texas, USA

Key Words. Debrided skin • Adipose stem cells • Burn wounds • Perivascular niche

ABSTRACT

Major traumatic injuries to the body, such as large surface area burns, limit the availability of autologous stem cell populations for wound repair. This report demonstrates that even after severe burn trauma to the body, resident stem cells present within the subcutaneous adipose tissue survive and are available for therapeutic uses. Debrided skin from wounded areas contains subcutaneous adipose tissue and can yield approximately 1.5 × 10^5 to 2.5 × 10^5 cells per milliliter of tissue. This observation indicates that tissue, which is normally discarded, could be a valuable source of stem cells. Initial immunohistochemistry of the debrided tissue localized platelet-derived growth factor receptor beta$^+$ (PDGFR-β^+) cells to perivascular niches of vascular beds. It was immunophenotypically confirmed that the cell isolates are stem cells and designated as debrided skin adipose-derived stem cells (dsASCs). Gene expression analysis of stem cell specific transcripts showed that the dsASCs maintained their stemness over serial passages. Furthermore, dsASCs were able to differentiate into adipogenic, osteogenic, and vascular cell lineages. Finally, an in vivo excision wound model in athymic rats demonstrated that the dsASCs are engrafted within a wound bed after 12 days. These data provide the first evidence that subcutaneous adipose tissue from discarded burned skin contains a viable population of stem cells that can be used for wound repair and skin regenerative therapies. STEM CELLS *2011;29:1219–1230*

Disclosure of potential conflicts of interest is found at the end of this article.

INTRODUCTION

Burn wounds constitute 5%–10% of military casualties, involving 40%–60% of total body surface area (TBSA) [1–3], and require extensive reconstruction [4, 5]. Stem cells, a valuable tool in regenerative medicine, have demonstrated the capacity to help heal extensively injured tissues [6, 7]. Among adult mesenchymal stem cells (MSCs), adipose-derived stem cells (ASCs) have gained particular attention due to their ease of isolation, relative abundance [8–12], and multilineage differentiation potential [13–19]. Recent studies of various tissues, including adipose tissue, indicate that their resident stem cell niches localize to perivascular regions and express markers of both MSCs (CD105, STRO-1, and CD34) and pericytic (NG2 and platelet-derived growth factor receptor beta (PDGFR-β)/CD140b) lineages [20–24]. These perivascular cells are in direct contact with the inner endothelium and help initiate a stable vessel network during angiogenic responses. Furthermore, this perivascular-endothelial cell interaction is necessary for restoring an appropriate microenvironment for tissue remodeling during skin regeneration [25].

After a burn injury, the host immediately responds by coordinating molecular signals to initiate healing of the wounded area [26]. Adipose tissue in conjunction with the host immune system plays an important role in initiating the signaling events in the healing process [27–29]. ASCs have demonstrated their capacity to elicit a “regenerative” response through autocrine, paracrine, or direct cell-cell interactions [30–34]. Unfortunately, after a severe burn injury, the source of autologous stem cells from a patient is restricted due to limited clinical access of normal stem cell sources (e.g., subcutaneous lipoaspirate) and the lack of uninjured viable tissue, requiring an alternate source of stem cells for regenerative approaches.

Current standard of care for burn injuries involves surgical debridement of necrotic tissue associated with eschar, followed by the application of skin grafts or tissue-engineered skin substitutes using allogeneic and/or autologous cells [35, 36]. The process of wound debridement typically involves the removal of subcutaneous layers and associated tissue structures, including portions of intact hypodermal adipose tissue. Based on this observation, we hypothesize that the intact adipose tissue associated with the debrided skin could be a source of viable autologous stem cells for use in wound

Disclaimer: The opinions and assertions contained herein are the private views of the authors and are not to be construed as official or reflecting the views of the Department of Defense or Department of Army. The authors are employees of the U.S. government, and this work was prepared as part of their official duties. This research was funded by the U.S. Army Medical Research and Materiel Command.

Author contributions: S.N.: conception and design, collection and assembly of data, manuscript writing, data analysis and interpretation; N.L.W.: collection and assembly of data, data analysis and interpretation; D.G.B.: conception and design, manuscript writing; R.J.C.: conception and design, data analysis and interpretation, manuscript writing.

Correspondence: Robert J. Christy, Ph.D., Extremity Trauma Research/Regenerative Medicine, United States Army Institute of Surgical Research, 3698 Chambers Pass, Bldg 3611-BHT1, Fort Sam Houston, TX 78234-6315, USA. Telephone: 210-539-9528; Fax: 210-539-3877; e-mail: robert.christy@us.army.mil Received January 12, 2011; accepted for publication May 24, 2011; first published online in STEM CELLS *EXPRESS* June 14, 2011. © AlphaMed Press 1066-5099/2009/$30.00/0 doi: 10.1002/stem.677

Report Documentation Page

Form Approved
OMB No. 0704-0188

Public reporting burden for the collection of information is estimated to average 1 hour per response, including the time for reviewing instructions, searching existing data sources, gathering and maintaining the data needed, and completing and reviewing the collection of information. Send comments regarding this burden estimate or any other aspect of this collection of information, including suggestions for reducing this burden, to Washington Headquarters Services, Directorate for Information Operations and Reports, 1215 Jefferson Davis Highway, Suite 1204, Arlington VA 22202-4302. Respondents should be aware that notwithstanding any other provision of law, no person shall be subject to a penalty for failing to comply with a collection of information if it does not display a currently valid OMB control number.

1. REPORT DATE **01 AUG 2011**	2. REPORT TYPE **N/A**	3. DATES COVERED **-**
4. TITLE AND SUBTITLE **Debrided skin as a source of autologous stem cells for wound repair**		5a. CONTRACT NUMBER 5b. GRANT NUMBER 5c. PROGRAM ELEMENT NUMBER
6. AUTHOR(S) **Natesan S., Wrice N. L., Baer D. G., Christy R. J.,**		5d. PROJECT NUMBER 5e. TASK NUMBER 5f. WORK UNIT NUMBER
7. PERFORMING ORGANIZATION NAME(S) AND ADDRESS(ES) **United States Army Institute of Surgical Research, JBSA Fort Sam Houston, TX**		8. PERFORMING ORGANIZATION REPORT NUMBER
9. SPONSORING/MONITORING AGENCY NAME(S) AND ADDRESS(ES)		10. SPONSOR/MONITOR’S ACRONYM(S) 11. SPONSOR/MONITOR’S REPORT NUMBER(S)
12. DISTRIBUTION/AVAILABILITY STATEMENT **Approved for public release, distribution unlimited**		
13. SUPPLEMENTARY NOTES		
14. ABSTRACT		
15. SUBJECT TERMS		

16. SECURITY CLASSIFICATION OF:			17. LIMITATION OF ABSTRACT	18. NUMBER OF PAGES	19a. NAME OF RESPONSIBLE PERSON
a. REPORT **unclassified**	b. ABSTRACT **unclassified**	c. THIS PAGE **unclassified**	**UU**	**12**	

Standard Form 298 (Rev. 8-98)
Prescribed by ANSI Std Z39-18

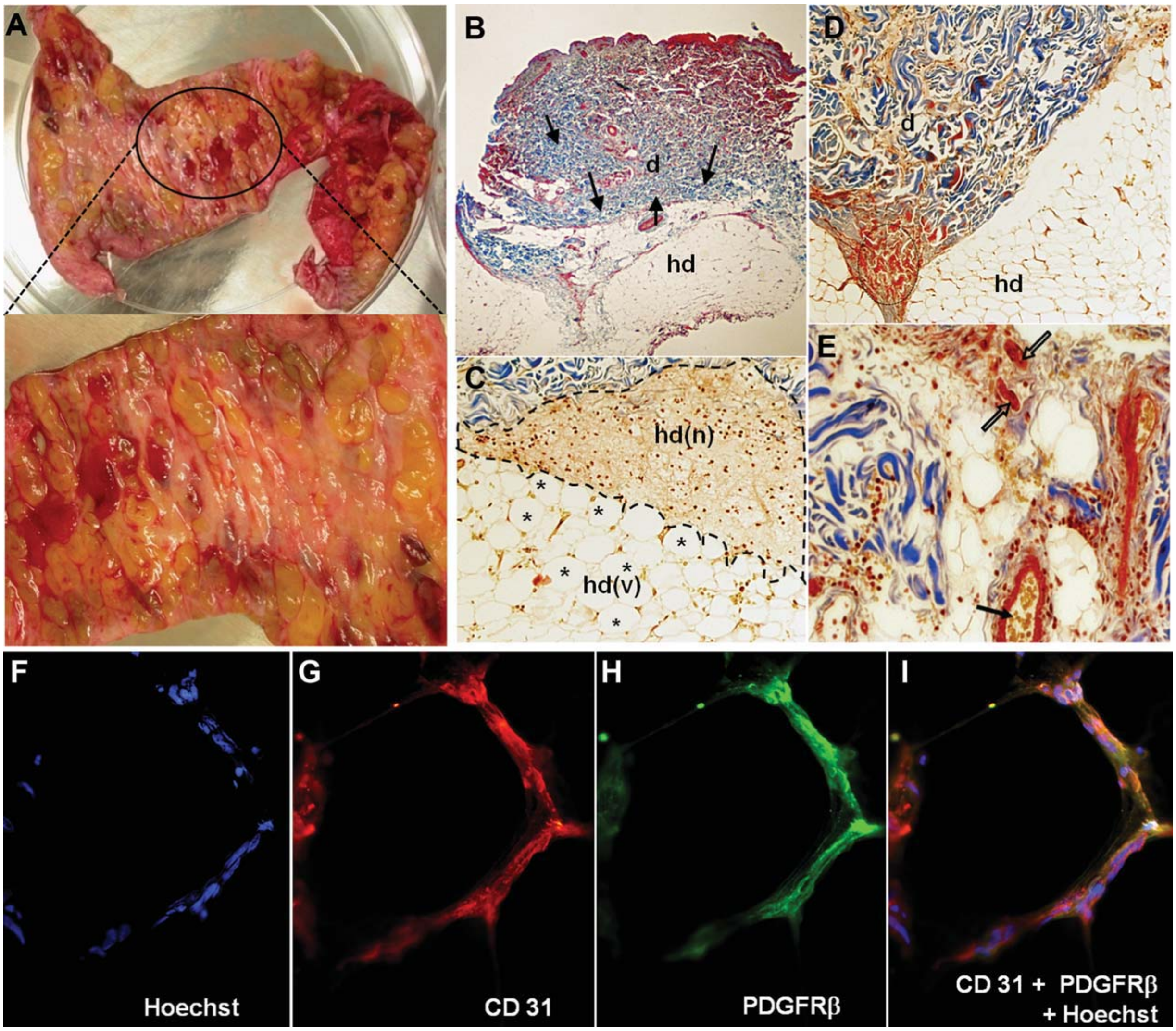

Figure 1. Discarded human skin after burn wound debridement. (**A**): Gross morphology of debrided tissue. (**B–E**): Histological analysis of sections stained with Masson's trichrome showing regions of (**B**): Necrotic dermis and hyalinized collagen (bold arrows). (**C**): Viable subcutaneous hypodermis regions with intact interlobular septae (asterisk) and other regions of completely necrotized tissue (serrated circle). (**D**): Thrombi were present at the dermal-hypodermal junction (serrated circle). (**E**): Other regions exhibited collapsed (open arrow) and patent blood vessels (closed arrow) in hypodermis. (**F–I**): Immunohistochemical analysis of microvessels in a discarded burn tissue stained with (**F**): Hoechst for nuclei. Primary antibodies for (**G**): CD31 (Alexa fluor 594) and (**H**): PDGFR*β* (Alexa fluor 488). (**I**): Overlay of CD31, PDGFR*β*, and Hoechst. Original magnification: ×40 (**B**), ×100 (**C, D**), ×200 (**E**), and ×400 (**F–I**). Abbreviations: *, viable subcutaneous hypodermis regions with intact interlobular septae; d, necrotic dermis; hd, hypodermis; hd(n), necrotic subcutaneous hypodermis; hd(v), viable subcutaneous hypodermis; PDGFR*β*, platelet-derived growth factor beta.

treatments. This study determined that (a) the hypodermal adipose region of the discarded human skin, after burn wound debridement, contains viable stem cells; (b) the cells appear to be of perivascular origin; and (c) the cells can be easily isolated and expanded in vitro and retain their ability to differentiate into multilineages. Furthermore, using an athymic rat excision wound model, we demonstrate that these cells can engraft into healing wound tissue.

MATERIALS AND METHODS

Discarded Human Burned Skin

Discarded human skin samples (Fig. 1A) from severely burned patients undergoing wound debridement were obtained from the Brooke Army Medical Center Burn Unit (Fort Sam Houston, TX). Samples were collected from 21 male burn patients with a mean age of 33 years. This study focused on the 20- to 30-year-old age group, which is the average age of military male burn patients [37]. From this age group, three samples were randomly selected for extensive analysis; and a sample from an older patient (age 49 years) was analyzed for age comparison (Table 1). This study was conducted under a protocol reviewed and approved by the U.S. Army Medical Research and Materiel Command Institutional Review Board and in accordance with the approved protocol (HSC20080290N). In this study, the authors were blinded from the patient information regarding TBSA and the status of the wound during surgical debridement. Before tissue processing, punch biopsies of approximately 5 mm in diameter were taken from various regions of the debrided sample and fixed with 10% neutral-buffered formalin for histological analysis or were cryopreserved for immunohistochemical analysis using the gradient sucrose cryopreservation technique [38].

Table 1. Debrided tissue samples

Patient	Age (years)	Percentage of tissue viability	dsASC yield floating fraction (cells per milliliter)
BH1	24	45	1.85×10^5
BH2	26	75	2.48×10^5
BH3	49	40	1.5×10^5
BH4	24	80	2.2×10^5

Histological Analysis

Histological analysis was performed on 5–7 μm sections of formalin-fixed biopsies from the discarded human skin samples and the granulation tissue collected from the wound bed of athymic rats. A "blinded" trained pathologist analyzed Masson's trichrome and/or H&E stained sections of the discarded human skin biopsies to assess tissue viability and burn depth and the overall wound healing pattern of the athymic rat tissue.

Isolation and Cell Culture

Discarded human skin samples were washed three times with Hanks' balanced saline solution (HBSS; Invitrogen, Carlsbad, CA, http://www.invitrogen.com/) to remove adherent blood clots. The hypodermal layer was dissected from the dermal region along with the areolar connective tissue, transferred to a petri dish, and then finely minced with scissors. The minced tissue was then suspended in HBSS (5 ml of minced tissue per 25 ml HBSS), centrifuged for 10 minutes at 500*g* at 16°C, and the floating fraction carefully pooled into sterile flasks. For every 1 ml of minced floating tissue, 3,500 units of collagenase type II (Sigma-Aldrich, St. Louis, MO, http://www.sigmaaldrich.com/) was added and incubated in an orbital shaker (125 rpm) for 45–60 minutes at 37°C. The digested tissue was filtered using 100 μm and 70 μm filters (BD Falcon, NJ, http://catalog.bd.com/) centrifuged at 500*g* for 10 minutes at 16°C and washed with lysing buffer (BD PharmLyse, BD Bioscience, San Jose, CA, http://www.bdbiosciences.com/) to remove any contaminating red blood cells. The remaining cell pellet was washed twice with sterile HBSS and resuspended in the following growth media: MesenPRO RS basal medium supplemented with MesenPRO RS growth supplement, antibiotic-antimycotic (100 U/ml of penicillin G, 100 μg/ml of streptomycin sulfate, and 0.25 μg/ml of Amphotericin B), and 2 mM L-glutamine (Invitrogen). Final cell isolates were cultured in flasks (2–2.6 $\times$ 10^4 cells per square centimeter, BD Falcon, NJ, http://catalog.bd.com/) and maintained in a 5% CO_2 humidified incubator at 37°C. After 4 hours in culture, the growth medium was replaced in the flasks to remove any floating debris. The remaining attached cells are designated as debrided skin ASCs (dsASCs). The capacity/ability of dsASCs to proliferate was assessed by counting the number of cells every 48 hours. After counting, 6×10^3 cells per square centimeter were replated and the process repeated for eight passages.

Immunohistochemical and Immunocytochemical Analysis

Cryosections of 10 μm from frozen biopsies were washed once with HBSS and fixed with 4% paraformaldehyde (PFA; EMS, Hatfield, PA, http://www.emsdiasum.com/) for 20 minutes at room temperature. After three washes with HBSS, nonspecific Fc receptor mediated sites were blocked by incubating the sections for 40 minutes with human Fc receptor blocking solution (Innovex Biosciences, Richmond, CA, http://www.innvx.com/), for 2 hours with 1% bovine serum albumin (BSA, Sigma) in HBSS, or 5% donkey serum (Sigma) for cytoskeletal markers. To localize cytosolic markers, sections were permeabilized with 0.01% Triton X-100 in HBSS and blocked for 2 hours with 1% BSA or 5% donkey serum. The human burn skin tissue sections were incubated with 10 μg/ml of anti-human monoclonal antibody directed against PDGFRβ (CD140b; BD Bioscience) and/or CD31 (R&D Systems, Minneapolis, MN, http://www.rndsystems.com/); tissue sections obtained on day 8 and 12 from rats treated with dsASC-Matrigel were incubated with 10 μg/ml human-specific antimitochondrial protein antibody (Millipore, Billerica, MA, http://www.millipore.com/) and 5 μg/ml mouse specific antilaminin monoclonal antibody (Millipore) to detect dsASCs and Matrigel within the wound bed, respectively. Tissue sections were incubated with primary antibodies overnight at 4°C. Primary antibodies were detected by incubating 5 μg/ml Alexafluor 488 and/or 594 (Invitrogen) tagged secondary antibodies of corresponding Ig class for 45 minutes at 4°C. Antibodies with product numbers are listed in Supporting Information Table 1.

Passage 1 (P1) dsASCs (BH1, BH2, and BH3) were cultured separately overnight in two-well chambered slides at 20,000 cells per well (Nalgene Nunc, LabTek chamber slide, Naperville, IL, http://www.nuncbrand.com/). The cells were washed twice with HBSS, fixed with 4% PFA for 20 minutes, and incubated overnight at 4°C with anti-human monoclonal antibodies targeted against transferrin receptor (CD71; 10 μg/ml R&D Systems), intercellular cell adhesion molecule-1 (CD54; 15 μg/ml R&D Systems), endoglin (CD105; 40 μg/ml R&D Systems), STRO-1 (20 μg/ml; R&D Systems), Thy-1 (CD90; 10 μg/ml BD Bioscience), and PDGFRβ (50 μg/ml, BD Bioscience). The specificity of human-specific antimitochondrial protein antibody (Millipore) was assessed in vitro by labeling dsASCs cocultured with rat ASCs (rASCs). rASCs were isolated by using a protocol described previously [12]. The tissue isolation was performed in compliance with the Animal Welfare Act and Animal Welfare Regulations and in accordance with the principles of the Guide for the Care and Use of Laboratory Animals. rASCs were cytoplasmically labeled with quantum dot (Qdot) nanocrystals 625 using Qtracker cell labeling kit (Invitrogen) according to the manufacturer's instructions. The rASCs and dsASCs were cultured in two-well chamber slides (20,000 cells per well), either alone or mixed in equal numbers (10,000 cells of each) for 48 hours. The cells were fixed with 4% PFA and immunolabeled with 5 μg/ml of monoclonal human-specific antimitochondrial protein antibody (Millipore). Primary antibody was detected using 5 μg/ml of Alexafluor 488 labeled secondary antibodies. After tissue sections and cells were processed for immunochemistry, their nuclei were stained with Hoechst 33,342 (10 μg/ml, Invitrogen) for 20 minutes at room temperature. Nonspecific fluorescence was determined by incubating cell preparations/tissue sections with isotype controls or solely with secondary labeled antibodies.

Flow Cytometry

P1 dsASCs from patients BH1–BH4 were washed twice with HBSS, trypsinized, and resuspended in fluorescence-activated cell sorting (FACS) cell staining buffer (Biolegend, San Diego, CA, http://www.biolegend.com/) to a final concentration of 5×10^5 cells per milliliter. The dsASCs were then incubated for 45 minutes (4°C) with fluorophore-labeled mouse anti-human antibodies (5–10 μg/ml): CD45-PE, CD90-PE, CD105-PE, and STRO-1-Alexa fluor 647 (Biolegend); CD54-FITC and CD71-PE (R&D Systems); PDGFRβ-PE (BD Bioscience); and CD19 and CD44 (R&D Systems). Experiments were controlled by incubating the dsASCs with their respective fluorophore-labeled isotype antibodies (10 μg/ml, R&D Systems). FACS analysis was performed with an FACS Aria flow cytometer (BD Bioscience). Data collected from P1 dsASC cultures were controlled by analyzing P0 cells from one preparation (BH2) to eliminate any biased results that may have occurred due to selective culture adherence of P1 cells. Commercially available ASCs from subcutaneous fat tissue (ZenBio Inc., Research Triangle Park, NC, http://www.zen-bio.com/) was used as a positive control. Before FACS analysis, forward and side scatter were adjusted for each sample using appropriate unstained cells to eliminate dead cells and cell debris. Autofluorescence signals were eliminated by adjusting the signal outputs from designated channels, and the sensitivity was adjusted to collect a gated population of cells. Total percentage of cells staining positive for individual markers within the gated populations was determined. Results were quantitated by FACS Diva software (BD Biosciences). Approximately 20,000 events were collected and analyzed to determine the total population of cells staining positive for cell surface specific markers.

Adipogenic, Osteogenic, and Vasculogenic Differentiation of dsASCs

P1 dsASCs were cultured to confluence and induced to differentiate toward adipogenic and osteogenic lineages, using methods described previously [39]. Adipogenic cells were stained for neutral lipids using oil red O (Sigma) and osteogenic cells for calcium phosphate deposition with Alizarin red S (Sigma). Tube formation assays were performed using 1.5 ml of growth factor-reduced Matrigel (BD Bioscience) in six-well culture inserts (BD Falcon). P2 dsASCs (50,000 cells per well) were added on top of the three-dimensional Matrigel and cultured for 10 days using the Cascade 200 medium containing growth supplements (Invitrogen), with/without 50 ng/ml of vascular endothelial growth factor (VEGF; Peprotech, NJ, http://www.peprotech.com/) and 10 ng/ml of basic fibroblast growth factor (bFGF; Peprotech); and a phase-contrast photomicrograph was taken. After differentiation, RNA was isolated to analyze the cells' ability to express adipogenic, osteogenic, and vasculogenic specific mRNA targets. Undifferentiated dsASCs were used as controls.

RNA Isolation and RT-PCR

Total RNA was isolated using Trizol LS reagent (Invitrogen) [40]. The concentration of RNA was determined at $OD_{260/280}$ using a NanoDrop spectrometer (NanoDrop Technologies, Inc., Wilmington, DE, http://www.nanodrop.com/). cDNA was synthesized in duplicate samples using 150 ng of total RNA to begin first-strand synthesis (SuperScript III first-strand synthesis supermix with oligo-dT primers, Invitrogen). The following primer sets were used to evaluate the mRNA expression of specific markers for stem cells: *CD71*, *CD90*, *CD105*, *PDGFRβ*, and *CD45* (negative control); adipogenic cells, insulin-regulated glucose transporter-4 (*GLUT-4*), adiponectin, peroxisome proliferator-activated receptor gamma (*PPARγ*), and leptin; and osteogenic cells, alkaline phosphatase (ALP), and runt-related transcription factor 2 (*Runx2*). Master mixes with 200 nM forward/reverse primers and SYBR GreenER, qPCR supermix (Invitrogen), and each sample of synthesized cDNA template were analyzed by real-time polymerase chain reaction (RT-PCR) using a Bio-Rad CFX96 thermal cycler system (Bio-Rad, Hercules, CA, http://www.bio-rad.com/). Nontemplate control and no reverse transcriptase controls were run for each reaction. Gene expression was normalized to glyceraldehye-3-phosphate dehydrogenase, and the fold change in expression levels for each mRNA transcript was determined by the $2^{-\Delta\Delta CT}$ method [41]. For the Matrigel (BD Bioscience) assays, RNA from five gels was pooled, and cDNA was synthesized as described. Expression levels of endothelial (*CD31*) and pericyte (*NG2*) specific genes were analyzed.

The fold change in expression levels for stem cell specific genes from P1 dsASCs was normalized to the expression levels of control ASCs (ZenBio Inc.). The fold change in expression levels for stem cell specific genes from P2 to P7 dsASCs was normalized to the expression levels of the corresponding P1 dsASCs. The fold change in expression of adipogenic, osteogenic, and vasculogenic differentiation specific genes was normalized to the expression levels of undifferentiated P2 dsASCs. All primer sets were designed by, and are proprietary to, SA Biosciences (Frederick, MD, http://www.sabiosciences.com/).

Engraftment of dsASCs In Vivo

Male *rnu* nude athymic rats (175–250 g) were obtained from Harlan Laboratories (Indianapolis, IN, http://www.harlan.com/) and housed in the United States Army Institute of Surgical Research animal care facility. Rats were allowed access to water and chow ad libitum. Before the wound was created, a silicone splinting ring was stapled around the delineated wound margin; and a 1.4-cm-diameter full-thickness excision wound was created on the dorsum down to the panniculus of rat [42, 43]. Animals were randomly divided into three groups of five: saline control (250 μl), Matrigel (1 ml), and Matrigel (1 ml) + 100,000 dsASCs (P2) isolated from patient BH3. All the wounds were dressed with Tegaderm transparent film dressing (3M, St. Paul, MN, http://www.3m.com/) and observed for up to 12 days. The wound beds, including the healed area of skin surrounding the wound, were harvested on days 8 and 12 and samples prepared for histological and immunohistochemical analysis.

RESULTS

Viability of Discarded Human Skin

Histological examination of Masson's trichrome and/or H&E stained biopsies of each debrided skin sample indicated that the debrided samples ranged from 40%–80% tissue viability (Table 1). Representative light micrographs of Masson's trichrome-stained sections (Fig. 1) show complete loss of epidermis and reticular dermal regions (Fig. 1B). The remnant dermal tissue shows the presence of hyalinized collagen (bold arrows) with loss of individual collagen bundles and cellular necrosis. The hypodermal region consisted of intact adipocytes separated by intact interlobular septae and thermally collapsed areas with complete necrosis of both fat cells and dermis (Fig. 1C). Some regions of tissue exhibited a loss of vascular patency and the presence of thrombi in the dermal-hypodermal junction (Fig. 1D). Still other regions of the tissue contained completely intact blood vessels (Fig. 1E).

Immunoflourescence analysis of frozen tissue biopsies showed the presence of PDGFRβ^+ cells (Fig. 1H) in the perivascular space of CD31$^+$ microvascular structures (Fig. 1G) in all four samples studied. Figure 1I shows a representative immunofluorescence image of PDGFRβ^+ cells specifically wrapping CD31$^+$ cells, which is observed throughout the hypodermal region, regardless of the burn severity. However, most of the PDGFRβ^+ cells appeared to be associated with intact microvessels. Although positively stained cells were observed in areas of collapsed lobular regions, a spatially distinct staining was not observed (data not shown).

Stem Cells from the Hypodermis of Debrided Skin

During cell isolation, hypodermis from all the debrided burn samples were separated into two fractions: a floating fraction, comprising most of the viable fat tissue, and a pellet fraction, composed of mostly extracellular components associated with some hypodermis and remnant dermal debris. The cells isolated from the floating fraction of debrided tissue were plated overnight, and all the adherent cells (dsASCs) were considered P0. A portion of the P0 cells were grown in chamber slides for 24–48 hours (P1; Fig. 2A) for morphological and immunocytochemical analysis. The cells exhibited characteristic fibroblast-like morphology and stained positive for stem cell-associated surface markers including CD54, CD71, CD90, CD105, STRO-1, and PDGFRβ (Fig. 2C). This demonstrates that the floating fraction of isolated cells is originated from the perivascular space of blood vessels surrounding the adipocytes. The P1 cells were negative for endothelial (CD31) and leukocytic (CD45) cell markers, indicating selective adherence of stem cells during subsequent subculture (data not shown). The floating hypodermal fraction, after collagenase digestion, yielded between 1.5×10^5 and 2.5×10^5 stem cells per milliliter, shows that cells could still be harvested irrespective of the skin tissue viability (Table 1). When the

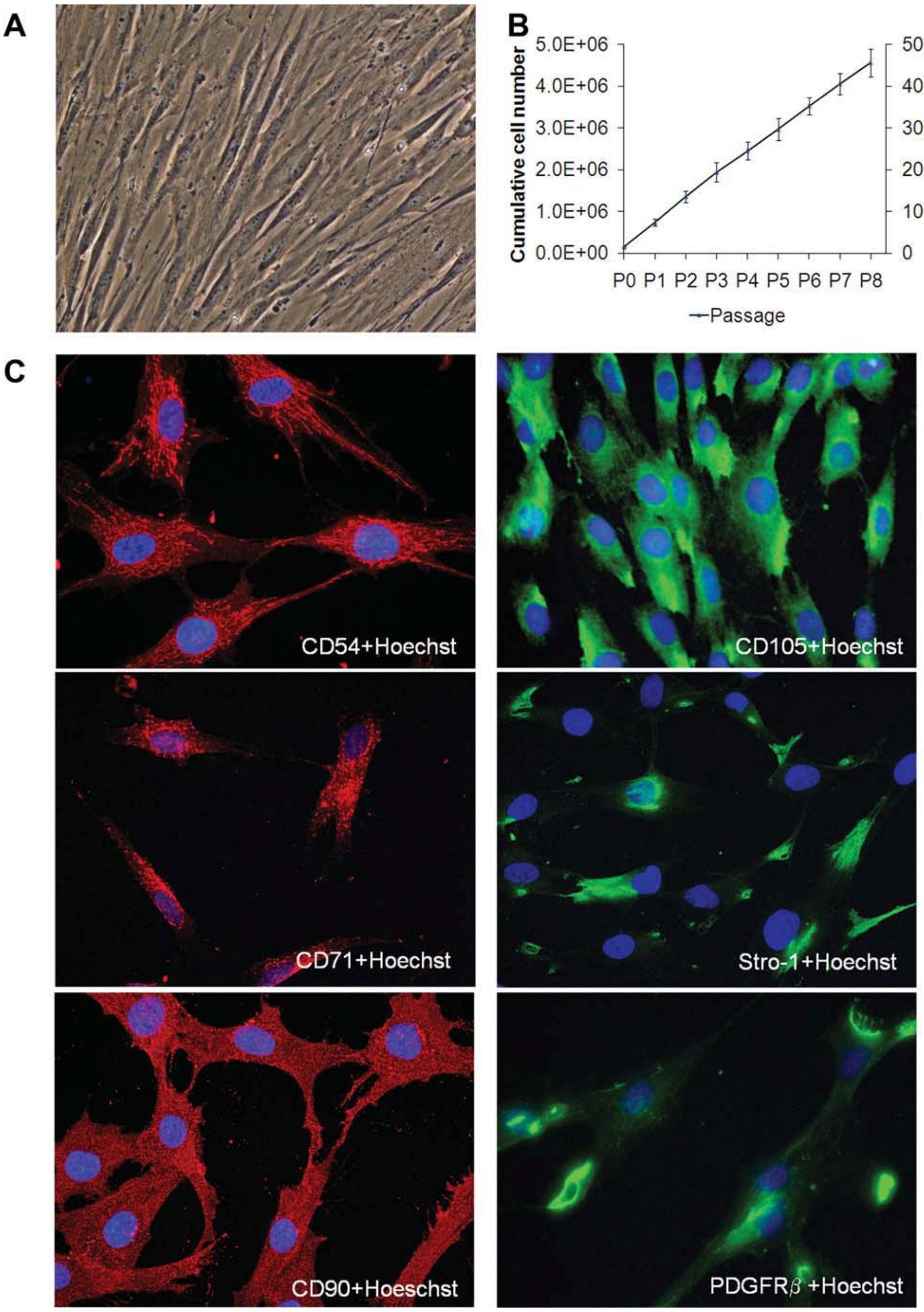
A
B
Cumulative cell number
5.0E+06
4.0E+06
3.0E+06
2.0E+06
1.0E+06
0.0E+00
Time (Hours)
500
400
300
200
100
0
P0 P1 P2 P3 P4 P5 P6 P7 P8
Passage
C
CD54+Hoechst
CD105+Hoechst
CD71+Hoechst
Stro-1+Hoechst
CD90+Hoeschst
PDGFRβ +Hoechst

Figure 2. Immunophenotype characterization of isolated debrided skin adipose-derived stem cells (dsASCs). **(A):** Micrograph depicting a confluent monolayer of dsASCs at Passage 1 (P1) isolated from the remnant hypodermis of debrided skin. **(B):** Cumulative cell number of dsASCs serially passed with an initial seeding density of 6×10^3 cells per square centimeter surface area. **(C):** Micrographs of dsASCs at P1, immunolabeled for stem cell surface markers CD54, CD71, and CD90 (Alexa fluor 594), CD105, STRO-1, and PDGFRβ (Alexa fluor 488). Nuclei were stained with Hoechst's reagent. Original magnification: ×200 **(A)** and ×400 **(C)**.

adherent cells obtained from the floating hypodermal fraction were subjected to serial passage, the dsASCs showed a four- to fivefold increase in cell number every 48 hours up to P4, after which the proliferation rate marginally decreased to three- to fourfold every 48 hours up to P8 (Fig. 2B).

FACS analysis (Fig. 3A) of P1 cells exhibited forward and side scatter plots consistent with the cell isolate having minimal contaminating $CD45^+$ cells (1%–3% ± 0.25, $n = 4$), which demonstrated that the isolation technique eliminated leukocytic contamination. The gated R1 population was $CD54^+CD71^+CD90^+CD105^+STRO\text{-}1^+$ for each patient sample. These cells were also PDGFRβ^+ (BH1, 87.8%; BH2, 79.6%; BH3, 69.4%; and BH4, 80.4%), suggesting their perivascular origin (compare with Fig. 1I). Overall, the percentage expression of CD71, CD90, CD105, and PDGFRβ markers was consistently high in all the samples analyzed (Fig. 3B) and not related to the percentage viability of the debrided tissue. $CD54^+STRO\text{-}1^+$ cell fractions were significantly lower for all the samples, when compared with $CD54^+CD71^+CD90^+CD105^+PDGFR\beta^+$ panel. All patient tissues used in this study were obtained from combat-associated burns; therefore, the patient pool consisted of mainly

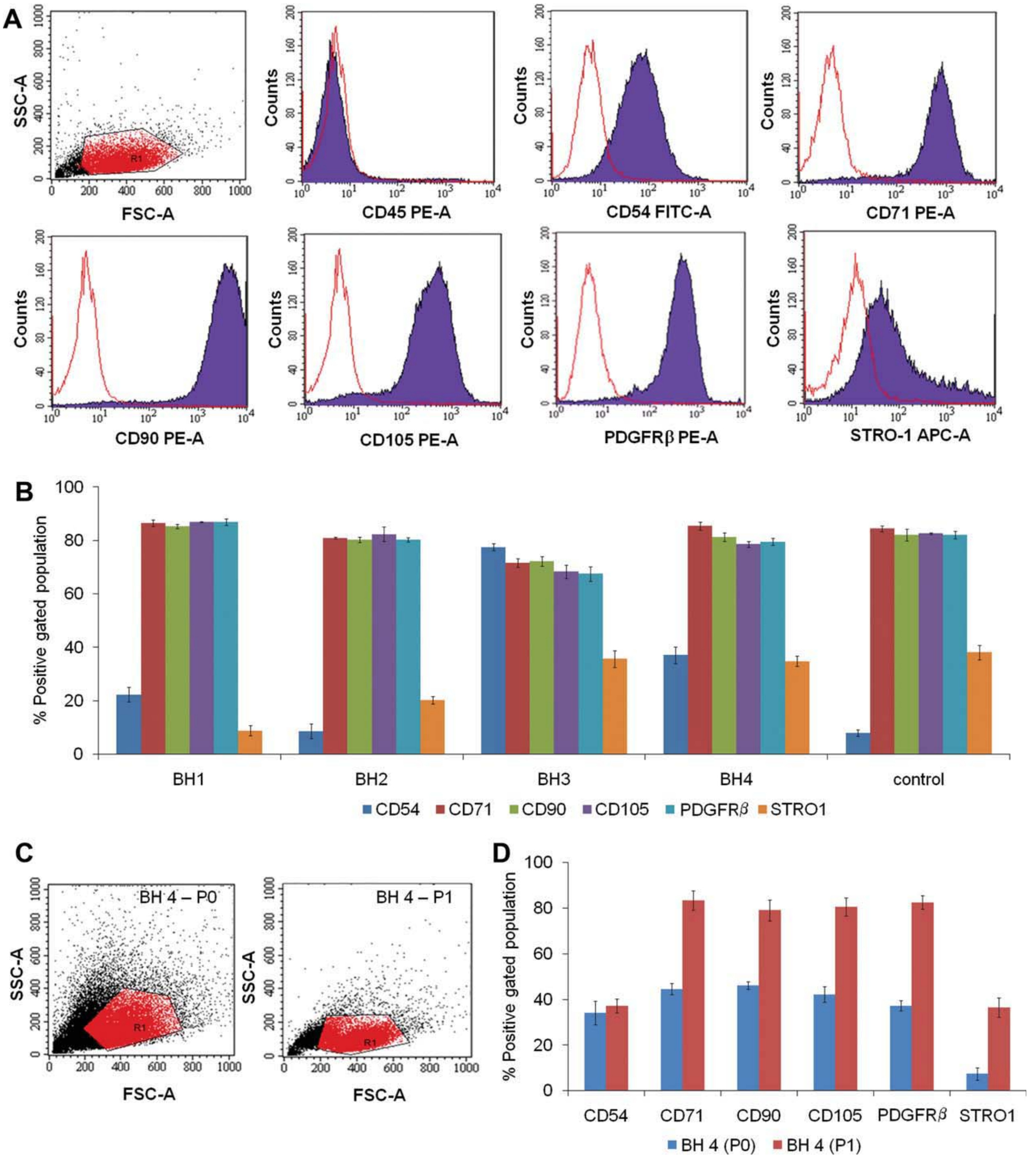

Figure 3. Fluorescence-activated cell sorting (FACS) analysis of debrided skin adipose-derived stem cells (dsASCs). The dsASC isolates from four different donors (BH1, BH2, BH3, and BH4) and control ASCs derived from a 32-year old healthy individual were analyzed for stem cell marker expression. **(A):** The top panel depicts scatter plots of Passage 1 (P1) dsASCs and FACS histograms for labeled antibodies specific for stem cell surface markers: CD45, CD71, CD90, CD105, PDGFR*β* (phycoerythrin), CD54 (flourescein isothyocynate), and STRO-1 (Alexa flour 647-APC). **(B):** Comparative bar graph of the percentage (±SD) gated population of dsASCs positive for CD54, CD71, CD90, CD105, PDGFR*β*, and STRO-1 in all four donor isolates and control ASCs. **(C):** FACS scatter plots showing the overall distribution of P0 and P1 dsASCs. **(D):** Bar graph of CD54, CD71, CD90, CD105, PDGFR*β*, and STRO-1 positive cells that were present within the total gated population of P0 and P1 dsASCs. For all FACS analysis, 20,000 events were collected ($n = 2$, percentage population ± SD) and analyzed for the total population positive for specific cell surface markers. The red line plot in all the FACS histograms represents isotype-matched antibody controls. Abbreviations: APC, allophycocyanin; FITC, flourescein isothyocynate; FSC, forward scatter; PE, phycoerythrin; PDGFR*β*, platelet-derived growth factor beta; SSC, side scatter.

young males. For this reason, positive control ASCs (Zenbio, Inc.) were isolated from subcutaneous fat of a younger, healthy adult male (age 32 years). In addition, dsASCs isolated from a 49-year-old patient was used for age comparison. Further investigation into the factors responsible for the age-related percentage change in number of stem cells for the panel of $CD54^{+}CD71^{+}CD90^{+}CD105^{+}PDGFR\beta^{+}$ markers is warranted.

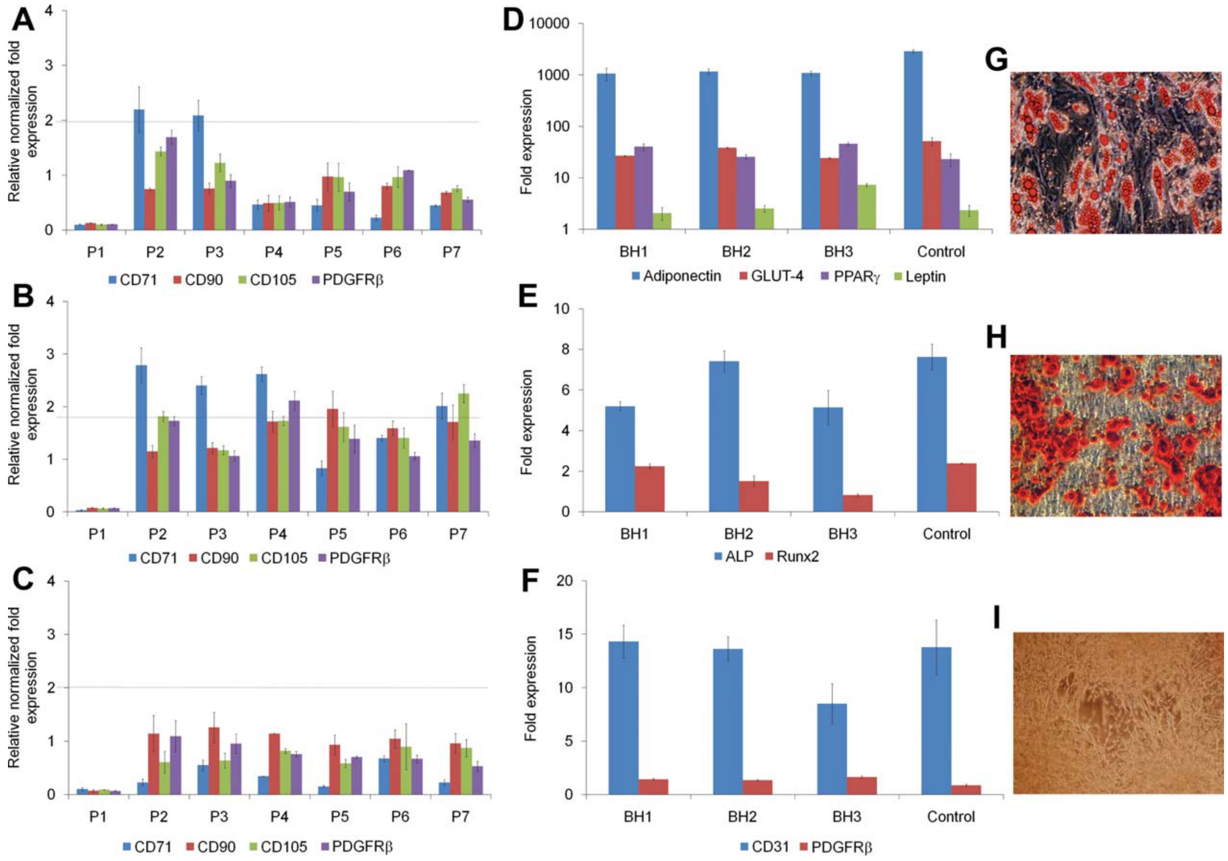

Figure 4. Debrided skin adipose-derived stem cells (dsASCs) passage and induction characterization. Real-time polymerase chain reaction (RT-PCR) analysis of stem cell specific markers *CD71*, *CD90*, *CD105*, and *PDGFRβ* in Passages P1–P7 dsASCs from BH1 **(A)**, BH2 **(B)**, and BH3 **(C)** donors. Expression levels of stem cell specific gene in P1 dsASCs are represented as mean fold change (±SD) of the normalized fold expression levels relative to positive control (P1 stem cells from subcutaneous adipose tissue of a healthy individual, Zenbio) and for passages P2–P7 (all the three patients), expression levels (mean fold change ± SD) of the above mentioned stem cell specific genes were calculated relative to the expression levels of their respective P1 cells. P2 dsASCs from patients BH1, BH2, BH3, and control ASCs were induced toward multilineages using specified conditions and examined for differentiation markers by RT-PCR. **(D):** Adiponectin, glucose transporter-4, leptin, and peroxisome proliferator-activated receptor gamma transcripts were examined for adipogenic induction. Alkaline phosphatase and *Runx2* are examined for osteogenic induction **(E)** PDGFR*β* for stem cells and CD31 for endothelial induction **(F)**. In addition to specific medium, dsASCs were cultured over three-dimensional Matrigel for endothelial induction. Expression levels of adipogenic, osteogenic, and endogenic specific genes ($n = 3$) were normalized to the levels of specific gene expression relative to undifferentiated P2 dsASCs and is represented as mean fold change (± SD). The serrated line in **(A)**, **(B)**, and **(C)** shows genes with higher than equal to twofold change. Photomicrographs of adipogenic differentiated dsASCs stained with oil red O, showing accumulation of oil vesicles in the cytoplasm **(G)**, osteogenic differentiated dsASCs stained with Alizarin red S showing matrix deposition of calcium crystals **(H)**, and endothelial-like cellular network over three-dimensional Matrigel **(I)**. Original magnification: ×100 **(G)**, ×100 **(H)**, and ×40 **(I)**. Abbreviations: *ALP*, alkaline phosphatase; *GLUT-4*, glucose transporter-4; *PDGFRβ*, platelet-derived growth factor beta; *PPARγ*, peroxisome proliferator-activated receptor gamma; *Runx2*, runt-related transcription factor 2.

dsASCs Maintain Stemness

To preliminarily assess the ability of the dsASCs to maintain their stemness after passaging, P0 and P1 cells were compared by FACS analysis for stem cell marker expression (Fig. 3C). A twofold higher percentage of CD54$^+$CD71$^+$CD90$^+$CD105$^+$PDGFRβ^+STRO-1$^+$ cells was present within the total gated population of P1 cells (Fig. 3D). P0 cells had a noticeable number of side-scattered events due to a mixture of leukocytes (6.2%), which were significantly low in P1 cultures (<1%), suggesting that after plating CD45$^+$ cells are substantially eliminated. Further, the P1 cells were CD19$^-$CD44$^+$ (Supporting Information Fig. S1A–S1C) [44], providing evidence for preferential expansion of stem cells. When expanded in culture, a high percentage of dsASCs was PDGFRβ^+ (Supporting Information Fig. S1D, S1E), suggesting that the cells originated from the perivascular space, while maintaining their stem cell characteristics.

For a more extensive analysis of dsASCs to maintain their stemness, gene expression levels of stem cell markers were studied using RT-PCR. Relative expression levels of *CD71*$^+$*CD90*$^+$*CD105*$^+$*PDGFRβ*$^+$ panel were investigated in dsASCs at different passages (P1–P7) for all the debrided tissue samples (Fig. 4A–4C). P1 cells exhibited little to no change in the expression levels for all the markers (less than 0.2-fold) regardless of age or percentage of tissue viability. In contrast, there was an apparent increase in the expression levels of *CD71*$^+$*CD90*$^+$*CD105*$^+$*PDGFRβ*$^+$ transcripts, with respect to tissue samples and passage number (P2–P7). dsASCs from BH1 and BH3, with 45% and 40% skin tissue viability, had variable gene expression levels during early passage (P2 and P3); whereas later-passage cells (P4–P7) showed fairly consistent levels of expression. In comparison, cells from BH2, which had 80% viability, showed consistent levels of elevated expression of stem cell markers throughout analysis.

P2 dsASCs from BH1, BH2, and BH3 also exhibited multilineage differentiation potential. When induced with adipogenic media, cytoplasmic accumulation of lipids began by

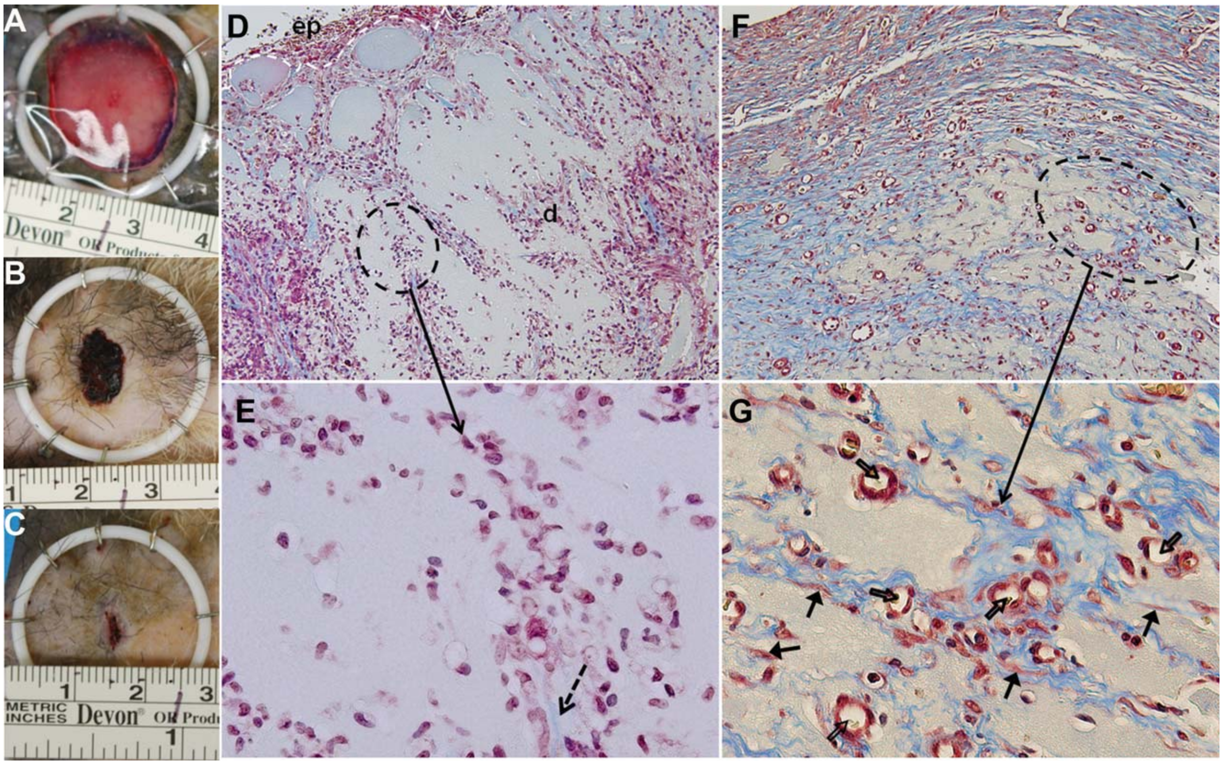

Figure 5. Engraftment of debrided skin adipose-derived stem cells (dsASCs) in rat model of skin wound healing. Excision wounds were treated with a mixture of dsASCs in Matrigel and the healing evaluated within the splinting ring. Wounds were covered with Tegaderm transparent film dressing and were examined on day 0 (**A**), day 8 (**B**), and day 12 (**C**). Days 8 and 12 were photographed with Tegaderm removed. Photomicrograph depicts a Masson's trichrome stained section of the healing wound with granulation tissue being formed on day 8 (**D**). The dotted white line shows the area above the granulated tissue being re-epithelialized. Higher magnification of granular substance in panel (**D**) (dotted black circle) shows the start of nascent collagen formation (**E**) (serrated arrow). Day 12 shows the presence of neocollagenous dermis (**F**) (dotted circle), while higher magnification of the same region shows the presence of blood vessels (open arrows) and fibroblast/myofibroblast like cells (closed arrows). Original magnification: ×100 (**D, E**), ×200 (**E**), and ×400 (**G**). Abbreviations: d, dermal layer; ep, epithelial layer.

day 6, and by day 14, when stained with oil red O, the cells showed intense red staining for lipids (Fig. 4G). Upon differentiation, the expression level of *PPARγ*, an early transcription promoting receptor factor [45], significantly increased in all samples (20–40-fold) and is similar to those observed in control ASCs (e.g., BH2, 25.6-fold, and control ASCs, 23.1-fold). Furthermore, the increase in adiponectin transcript levels (approximately 1,000-fold) demonstrates the ability of dsASCs to undergo adipogenesis through the activation of a glucose-regulated signaling pathway [46]. In addition, expression of *GLUT-4* and leptin from all patient samples was significantly higher relative to noninduced dsASCs (Fig. 4D).

When dsASCs were differentiated into an osteogenic lineage, all samples showed increased expression levels of *ALP*, indicative of stromal cell commitment to osteogenesis [39], and showed comparable levels of expression as control ASCs. Matrix mineralization appeared by day 8 postinduction and increased over time, with the cells positively staining for calcium by day 21 (Fig. 4H). Terminal differentiation was confirmed by the expression of *Runx2*, a master osteogenic transcription factor responsible for mature osteoblast formation (Fig. 4E). Induced cells from all the patient samples and control ASCs expressed Runx2 by 21 days with subtle differences in each expression level. Still, faster osteogenic induction was observed in cells isolated from higher viable tissue (BH2) in comparison to those derived from less viable tissue (BH1 and BH3). Expression of *Runx2* significantly increased by 28 days (approximately 70-fold) along with *ALP* (approximately sevenfold), indicating the commitment of dsASCs toward the osteogenic lineage (data not shown).

The ability of dsASCs to differentiate toward a vascular phenotype was also investigated. P2 dsASCs were seeded over a three-dimensional matrix of Matrigel and induced with endothelial cell-specific media. The dsASCs spontaneously joined, forming tubular structures covering the entire surface of the Matrigel, with a dense cellular network forming within 10 days (Fig. 4I). When analyzed by RT-PCR, the differentiated dsASCs from BH1, BH2, and BH3 exhibited a significant increase in expression of *CD31* (Fig. 4F) when compared with undifferentiated cells. Furthermore, the expression levels of *PDGFRβ* did not change, revealing that under endogenic induction conditions, dsASCs differentiate into endothelial-like cells rather than pericytic cells. The differentiated cells from all the samples, regardless of percentage viability, show negligible increases in expression levels of the pericyte specific marker *NG2* (less than 0.1-fold, data not shown). These results are comparable to recent studies showing that ASCs seeded on Matrigel are capable of forming capillary tube-like networks in vitro but are unstable over time [23, 25].

In Vivo Engraftment of dsASCs

Engraftment efficiency of dsASCs (P2; BH2) was assessed using an excision wound splinting model [42] in immunodeficient rats (Fig. 5A). After 8 and 12 days postgrafting of dsASC-Matrigel composites, the wound bed was photographed (Fig. 5B, 5C) and harvested for analysis using routine histological examination. The dsASC-Matrigel composite integrated within the healing wound bed as depicted within the serrated black circles in Figure 5D, 5F, which corresponds to days 8 and 12, respectively. This was further confirmed

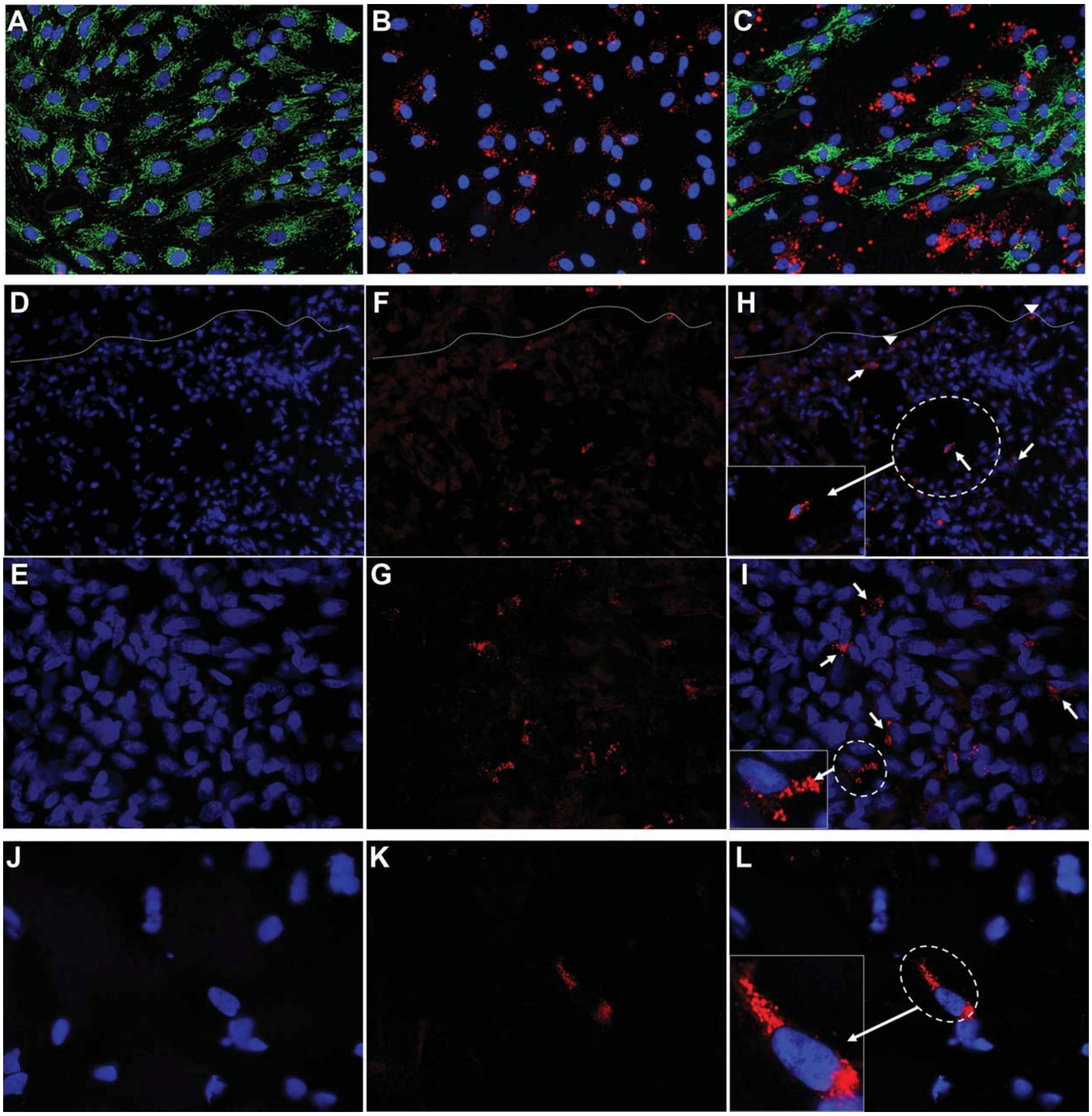

Figure 6. Tracking of human debrided skin adipose-derived stem cells (dsASCs) in vivo using a rat model of skin wound healing. To qualify the specificity of the human-specific anti-mitochondrial protein antibody, in vitro coculture experiments were performed using mixtures of rat ASCs (rASCs) and dsASCs. Immunofluorescence labeling of pure human dsASCs with the anti-human mitochondrial antibody **(A)** (green), and cultures of pure rASCs labeled with Q-dots **(B)** (red) were also subjected to the anti-human mitochondrial antibody **(B)** (negative). **(C):** Cocultures of an equal number of dsASCs and Qdot labeled rASCs immunostained with anti-human specific mitochondrial protein antibody demonstrates that the antibody specifically detects dsASCs and not rASCs. To examine the behavior of dsASCs in vivo in a rat model, wound beds were treated with a mixture of Passage 2 (P2) dsASCs in Matrigel (100,000 per wound) and tracked by staining with human-specific anti-mitochondrial protein antibody **(F, G, K)** (red), and total cells tracked by Hoechst stain (rat host and human dsASCs) in the wound bed **(D, E, J)** (blue). To simultaneously view both total cells and transplanted dsASCs in the same region, photomicrographs were superimposed as follows: **(D, F)** = **(H)**, **(E, G)** = **(I)**, **and (J, K)** = **(L)**. **(D–I)** Day 8 images; **(J–L)** day 12 images. Human cells were able to be detected in the wound bed (white arrows in **(H)** and **(I)**) and at the re-epithelializing surface (white arrow heads in **(H)**), surrounded by an acellular region (white serrated circle in **(H)**) on day 8. Higher magnification shows the dermal matrix populated with human dsASCs **(I)** (inset). Panel **(L)** inset shows multifocal punctate cytoplasmic staining of human mitochondrial staining observed on day 12. Serrated white line on panel **(D)**, **(F)**, and **(H)** shows the region of re-epithelialization (above the line). Original magnification: ×200 **(D, F, H)**, ×600 **(E, G, I)**, and ×900 **(J–L)**.

through positive staining of the wound bed for laminin (a major component of Matrigel) observed on day 8 (Supporting Information Fig. S2A–S2C) and on day 12 (Supporting Information Fig. S2D–S2F).

On day 8, the wound-composite region was rich in cells and lacked collagen bundles. Re-epithelialization was evident at the epidermal region (cells above the dotted white line in Fig. 5D) and loosely associated with the acellular amorphous matrix (Matrigel). The dermis showed the presence of multifocal amorphous matrices with organized fibrous granulation tissue along with spindle-shaped cells and nascent collagen (Fig. 5E), eventually turning into a mature vascularized wound bed by day 12 (Fig. 5F, 5G, blood vessels indicated by the open arrow in Fig. 5G). On day 12, a comparison of wound beds on rats treated only with Matrigel and no dsASCs showed predominantly acellular multifocal amorphous matrix (Supporting Information Fig. S3A, S3B) and was avascular (Supporting Information Fig. S3C), when compared with those treated with a dsASC-Matrigel mixture (Supporting Information Fig. S3D). In control rats, the wounds showed a normal progression of neodermis with vascularized fibrogranulation tissue formation (Supporting Information Fig. S3E, S3F).

dsASCs integrated within the healing wound bed were identified with human-specific antimitochondrial protein antibody [47]. The antibody specificity was assessed by immunofluorescence staining of a coculture of BH2 dsASCs and rASCs (Fig. 6A–6C) and the anti-mitochondrial protein antibody. Figure 6D, 6E, 6J represent Hoechst staining of rat and human cell nuclei present in the wound bed, with day 8 being depicted in Figure 6D, 6E and day 12 in Figure 6J. dsASCs are specifically identified in Figure 6F, 6G, 6K, with day 8 being depicted in Figure 6F, 6G and day 12 in Figure 6K. To colocalize both cell types simultaneously in the wound bed, images of the same area were obtained using separate fluorescence channels and images superimposed. Using this technique, it was determined that on day 8, a significant number of human cells was present throughout the dermal matrix (Fig. 6H, 6I, white arrow) with few cells residing at the re-epithelializing surface (white arrowheads were detected). At higher magnification, the dermal region showed immunopositive labeling for dsASCs (Fig. 6I and inset) surrounded by host cells (cells showing only nuclei staining). On day 12, dsASCs were visible in isolated, acellular regions of the wound-composite (Fig. 6H; white serrated circle). At day 12, very few human cells were localized in the wound bed, and those observed were mostly confined to the dermal region with multifocal punctate cytoplasmic fluorescence (Fig. 6L and inset).

DISCUSSION

This study provides evidence for a new source of autologous stem cells derived from discarded burn tissue after wound debridement. The dissected hypodermal layer is a practical source of autologous ASCs (1.5×10^5 and 2.5×10^5 stem cells per milliliter), which could be used for developing burn wound therapies. The viable cells isolated from debrided tissue were identified as stem cells (dsASCs) and have a similar panel of cell surface markers as ASCs isolated from a normal subcutaneous lipoaspirate [8]. Previous studies have shown that the cells comprising capillary vessels in adipose tissue exhibit spatially separated expression of CD31 and PDGFRβ markers [20]. These PDGFRβ^+ cells have been identified as the point of origin for isolated ASCs. These ASCs occupy the perivascular space and are immunopositive for stromal (CD44, CD90, CD105, and STRO-1) and pericytic (PDGFRβ, NG2, and 3G5) cell-specific markers [48, 49]. Our results indicate that the debrided skin biopsies possess both PDGFRβ^+ and CD31$^+$ cells and that isolated dsASCs (P1) are a relatively homogenous cell population when cultured in vitro. These dsASCs consistently express CD54$^+$CD71$^+$ CD90$^+$CD105$^+$PDGFRβ^+ markers in high percentages (>65%) regardless of tissue viability, with discernible variations in CD54 and STRO-1 expression. This observation is analogous to other studies, where culture expansion of clonally selected STRO-1$^+$CD31$^-$CD45$^-$ cells increases their multilineage differentiation capabilities [44, 50]. Furthermore, dsASCs from all samples were able to maintain stemness as demonstrated by their gene expression profile for stem cells markers when P1 dsASCs were compared with P1 ASCs derived from a healthy individual. The expression of these markers remained consistent across P1–P7 passages with little to no variability resulting from age difference of donors. This finding illustrates that the stemness of the isolated dsASCs remains unaffected after thermal injury to the surrounding tissue. Cells isolated from the youngest donor (BH1: approximately 45% tissue viability), when compared with older donors, exhibited higher expression levels of panel markers during initial passages than in later passages. These results imply that the expandability and the ability of dsASCs to maintain their stemness are directly dependent on patient age, an observation corroborated by other studies [51]. Similarly, of the various markers tested, CD71 has been shown to have a one- to twofold higher expression level in proliferating cells [52, 53]; this observation is dependent on passage number, patient age, and viability of debrided skin tissue. In our dsASCs cultures, relative expression levels of CD71 could be considered as an index to characterize the ability of culture-expanded dsASCs to maintain their stemness between donors. However, any effect that age may have on dsASCs stemness properties requires further investigation due to the lack of older patient burn samples in this study.

Furthermore, dsASCs exhibited adipogenic, osteogenic, and endothelial differentiation potential, confirming their stem cell-like phenotype. Regardless of age or viability of skin, dsASCs displayed adipogenesis through the classical pathway of transcription activation of adipogenic-specific genes involved in early (*PPARγ*) and terminal (leptin and adiponectin) stages of differentiation [45]. Increases in leptin, *GLUT-4*, and adiponectin transcript levels between days 14 and 21 were consistent with ASCs differentiation isolated from healthy individuals. When dsASCs were induced with osteogenic media, calcium deposition and increased levels of ALP and *Runx2* were observed, demonstrating commitment of dsASCs to undergo osteogenesis [54, 55]. It is noteworthy that Jackson et al. [56] and Nesti et al. [57] recently showed that mesenchymal progenitor cells isolated from traumatized muscle expressed similar sets of stem cell markers (expressed by dsASCs) in uninjured muscle tissue. Finally, we also show that dsASCs can be induced toward an endothelial phenotype when seeded on Matrigel, a characteristic feature of MSCs of pericytic origin [23]. This differentiation potential of dsASCs could be stimulated with exogenous mitogens, such as vascular endothelial growth factor and basic fibroblast growth factor, further confirming their ability to be induced toward an endothelial phenotype (data not shown). In this study, dsASCs were able to form tube-like networks across the three-dimensional Matrigel but became unstable after several days. This phenomenon demands further investigation to determine the role of dsASCs in forming both endothelial cells and pericytes during neovascularization both in vitro and in vivo.

When the dsASC-Matrigel mixture was applied to an excision wound in athymic rats, they engrafted into the granulating wound bed after 8 days, with only a few cells identified on day 12. The embedded dsASCs may be contributing significantly to the wound healing and skin regeneration process in this model, which complements the recent finding that ASCs do contribute to healing of chronic wounds [58]. Overall, the data reported in this study supports the hypothesis that dsASCs can be a source of stem cells for skin regenerative therapies, especially in patients with burn wounds involving large TBSA. In these patients, accessibility of autologous MSCs from normal tissue sources (e.g., bone marrow and lipoaspirates) is not feasible clinically. Therefore, in such cases, the hypodermal layer of discarded burn tissue may be an invaluable source of stem cells for wound repair and skin regeneration.

CONCLUSION

This study provides evidence that stem cells in the hypodermis are preserved during and after severe thermal injury. These autologous stem cells can be isolated from the debrided skin that is surgically removed from burn-injured patients and in quantities that could be useful clinically for burn repair and regeneration. Considering that large TBSA burn wounds require extensive debridement, this waste tissue represents an invaluable stem cell source. Promising results from both in vitro and in vivo perspectives support the use of dsASCs alone or in combination with appropriate bioscaffolds as a useful therapeutic tool in the field of regenerative medicine.

ACKNOWLEDGMENTS

We thank Cpt. Laura McGhee and Thomas Garza for collection of debrided tissue; Col. Seung Kim and Ltc. Scot J. Estep for their valuable suggestions and histopathological analysis of human and rat tissues samples; Dr. Shanmuganathan Seetharaman, Dr. David Zamora, Janet Roe, and Sharanda Hardy for their technical support; and Karla Moncada for providing technical support at the cell sorting core facility. This work was supported by the University of Texas Health Science Center at San Antonio and NIH Grant NCI P30 CA054174 (Cancer Therapy & Research Center). S.N. is supported by a Postdoctoral Fellowship Grant from the Pittsburgh Tissue Engineering Initiative (PTEI). This research was funded by the U.S. Army Medical Research and Materiel Command.

DISCLOSURE OF POTENTIAL CONFLICTS OF INTEREST

The authors indicate no potential conflicts of interest.

REFERENCES

1 Chung KK, Blackbourne LH, Wolf SE et al. Evolution of burn resuscitation in Operation Iraqi Freedom. J Burn Care Res 2006;27:606–611.

2 Wolf SE, Kauvar DS, Wade CE et al. Comparison between civilian burns and combat burns from Operation Iraqi Freedom and Operation Enduring Freedom. Ann Surg 2006;243:786–792.

3 White CE, Renz EM. Advances in surgical care: Management of severe burn injury. Crit Care Med 2008;36(suppl 7):S318–S324.

4 Owens BD, Wenke JC, Svoboda SJ et al. Extremity trauma research in United States Army. J Am Acad Orthop Surg 2006;14(suppl 10):S37–S40.

5 Bremner LF, Mazurek M. Reconstructive challenges of complex battle field injury. J Surg Orthop Adv 2010;19:77–84.

6 Picinich SC, Mishra PJ, Glod J et al. The therapeutic potential of mesenchymal stem cells. Cell- & tissue-based therapy. Expert Opin Biol Ther 2007;7:965–973.

7 Horwitz EM, Dominici M. How do mesenchymal stromal cells exert their therapeutic benefit? Cytotherapy 2008;10:771–774.

8 Aust L, Devlin B, Foster SJ et al. Yield of human adipose-derived adult stem cells from liposuction aspirates. Cytotherapy 2004;6:7–14.

9 Prunet-Marcassus B, Cousin B, Caton D et al. From heterogeneity to plasticity in adipose tissues: Site-specific differences. Exp Cell Res 2005;312:727–736.

10 Van Harmelen V, Rohrig K, Hauner H. Comparison of proliferation and differentiation capacity of human adipocytes precursor cells from the omental and subcutaneous adipose tissue depot of obese subjects. Metabolism 2004;53:632–637.

11 Wickham MQ, Erickson GR, Gimble JM et al. Multipotent stromal cells derived from the infrapatellar fat pad of the knee. Clin Orthop Relat Res 2003;412:196–212.

12 Zuk PA, Zhu M, Mizuno H et al. Multilineage cells from human adipose tissue: Implications for cell-based therapies. Tissue Eng 2001;7:211–228.

13 Brzoska M, Geiger H, Gauer S et al. Epithelial differentiation of human adipose tissue-derived adult stem cells. Biochem Biophys Res Commun 2005;330:142–150.

14 Bunnell BA, Estes BT, Guilak F et al. Differentiation of adipose stem cells. Methods Mol Biol 2008;456:155–171.

15 Dhar S, Yoon ES, Kachgal S, Evans GR. Long-term maintenance of neuronally differentiated human adipose tissue-derived stem cells. Tissue Eng 2007;13:2625–2632.

16 Di Rocco G, Iachininoto MG, Tritarelli A, Straino S, Zacheo A, Germani A, Crea F, Capogrossi MC. Myogenic potential of adipose-tissue-derived cells. J Cell Sci 2006;119:2945–2952.

17 Halvorsen YD, Franklin D, Bond AL et al. Extracellular matrix mineralization and osteoblast gene expression by human adipose tissue-derived stromal cells. Tissue Eng 2001;7:729–741.

18 Lin Y, Luo E, Chen X et al. Molecular and cellular characterization during chondrogenic differentiation of adipose tissue-derived stromal cells in vitro and cartilage formation in vivo. J Cell Mol Med 2005;9:929–939.

19 Planat-Benard V, Silvestre JS, Cousin B et al. Plasticity of human adipose lineage cells towards endothelial cells: Physiological and therapeutic perspectives. Circulation 2004;109:656–663.

20 Crisan M, Yap S, Casteilla L et al. A perivascular origin for mesenchymal stem cells in multiple human organs. Cell Stem Cell 2008;3:301–313.

21 Katz AJ, Tholpady A, Tholpady SS et al. Cell surface and transcriptional characterization of human adipose-derived adherent stromal (hADAS) cells. Stem Cells 2005;3:412–423.

22 Shi S, Gronthos S. Perivascular niche of postnatal mesenchymal stem cells in human bone marrow and dental pulp. J Bone Miner Res 2003; 18:696–704.

23 Traktuev DO, Merfeld-Clauss S, Li J et al. A population of multipotent CD34-positive adipose stromal cells share pericyte and mesenchymal surface markers, reside in a periendothelial location, and stabilize endothelial networks. Circ Res 2008;102:77–85.

24 Amos PJ, Shang H, Bailey AM et al. IFATS collection: The role of human adipose-derived stromal cells in inflammatory microvascular remodeling and evidence of a perivascular phenotype. Stem Cells 2008;26:2682–290.

25 Rubina K, Kalinina N, Efimenko A et al. Adipose stromal cells stimulate angiogenesis via promoting progenitor cell differentiation, secretion of angiogenic factors, and enhancing vessel maturation. Tissue Eng Part A 2009;15:2039–2050.

26 Paquet-Fifield S, Schlüter H, Li A et al. A role for pericytes as microenvironmental regulators of human skin tissue regeneration. J Clin Invest 2009;119:2795–2806.

27 Gurtner GC, Werner S, Barrandon Y et al. Wound repair and regeneration. Nature 2008;453:314–21.

28 Kopp A, Buechler C, Neumeier M et al. Innate immunity and adipocyte function: Ligand-specific activation of multiple toll-like receptors modulates cytokine, adipokine, and chemokine secretion in adipocytes. Obesity 2009;17:648–656.

29 Saillan-Barreau C, Cousin B, André M et al. Human adipose cells as candidates in defense and tissue remodeling phenomena. Biochem Biophys Res Commun 2003;309:502–505.

30 Kang SK, Jun ES, Bae YC et al. Interactions between human adipose stromal cells and mouse neural stem cells in vitro. Brain Res Dev Brain Res 2003;145:141–149.

31 Kim WS, Park BS, Sung JH et al. Wound healing effect of adipose-derived stem cells: A critical role of secretory factors on human dermal fibroblasts. J Dermatol Sci 2007;48:15–24.

32 Nakagami H, Maeda K, Morishita R et al. Novel autologous cell therapy in ischemic limb disease through growth factor secretion by cultured adipose tissue derived stromal cells. Arterioscler Throm Vasc Biol 2005;25:2542–2547.

33 Wang B, Han J, Gao Y et al. The differentiation of rat adipose-derived stem cells into OEC-like cells on collagen scaffolds by co-culturing with OECs. Neurosci Lett 2007;421:191–196.

34 Zaragosi L-E, Ailhaud G, Dani C. Autocrine fibroblast growth factor 2 signaling is critical for self-renewal of human multipotent adipose-derived stem cell. Stem Cells 2006;24:2412–2419.

35 Mansbridge JN. Tissue-engineered skin substitutes in regenerative medicine. Curr Opin Biotechnol 2009;20:563–567.

36 Supp DM, Boyce ST. Engineered skin substitutes: Practices and potentials. Clin Dermatol 2005;23:403–412.

37 Chapman TT, Richard RL, Hedman TL et al. Military return to duty and civilian return to work factors following burns with focus on the hand and literature review. J Burn Care Res 2008;29:756–762.

38 Barthel LK, Raymond PA. Improved method for obtaining 3-microns cryosections for immunocytochemistry. J Histochem Cytochem 1990; 38:1383–1388.

39 Zuk PA, Zhu M, Ashjian P et al. Human adipose tissue is a source of multipotent stem cells. Mol Biol Cell 2002;13:4279–4295.

40 Chomczynski P, Sacchi N. Single-step method of RNA isolation by acid guanidinium thiocyanate-phenol-chloroform extraction. Anal Biochem 1987;162:156–159.

41 Livak KJ, Schmittgen TD. Analysis of relative gene expression data using real-time quantitative PCR and the $2^{-\Delta\Delta CT}$ method. Methods 2001;25:402–408.

42 Chen L, Tredget EE, Liu C et al. Analysis of allogenicity of mesenchymal stem cells in engraftment and wound healing in mice. PLoS One 2009;4:e7119.

43 Galiano RD, Michaels J 5th, Dobryansky M et al. Quantitative and reproducible murine model of excisional wound healing. Wound Repair Regen 2004;12:485–492.

44 Mitchell JB, McIntosh K, Zvonic S et al. Immunophenotype of human adipose-derived cells: Temporal changes in stromal-associated and stem cell-associated markers. Stem Cells 2006;24:376–385.

45 Ntambi JM, Young-Cheul K. Adipocyte differentiation and gene expression. J Nutr 2000;130:3122S–3126S.

46 Fernyhough ME, Okine E, Hausman G et al. PPAR gamma and GLUT-4 expression as developmental regulators/markers for preadipocyte differentiation into an adipocyte. Domest Anim Endocrinol 2007; 33:367–378.

47 Swana GT, Swana MR, Bottazzo GF et al. A human-specific mitochondrial antibody its importance in the identification of organ-specific reactions. Clin Exp Immunol 1977;28:517–525.

48 Zannettino AC, Paton S, Arthur A et al. Gronthos S. Multipotent human adipose-derived stromal cells exhibit a perivascular phenotype in vitro and in vivo. J Cell Physiol 2008;214:413–421.

49 Yoshimura K, Shigeura T, Matsumoto D et al. Characterization of freshly isolated and cultured cells derived from the fatty and fluid portions of liposuction aspirates. J Cell Physiol 2006;208:64–76.

50 Gronthos S, Franklin DM, Leddy HA et al. Surface protein characterization of human adipose tissue-derived stromal cells. J Cell Physiol 2001;189:54–63.

51 de Girolamo L, Lopa S, Arrigoni E et al. Human adipose-derived stem cells isolated from young and elderly women: Their differentiation potential and scaffold interaction during in vitro osteoblastic differentiation. Cytotherapy 2009;11:793–803.

52 Tani H, Morris RJ, Kaur P. Enrichment for murine keratinocyte stem cells based on cell surface phenotype. Proc Natl Acad Sci USA 2000; 97:10960–10965.

53 Lorenz K, Sicker M, Schmelzer E et al. Multilineage differentiation potential of human dermal skin-derived fibroblasts. Exp Dermatol 2008;17:925–932.

54 Ducy P, Zhang R, Geoffroy V et al. Osf2/Cbfa1: A transcriptional activator of osteoblast differentiation. Cell 1997;89:747–754.

55 Jaiswal N, Haynesworth SE, Caplan AI et al. Osteogenic differentiation of purified, culture-expanded human mesenchymal stem cells in vitro. J Cell Biochem 1997;64:295–312.

56 Jackson WM, Lozito T, Djouad F et al. Differentiation and regeneration potential of mesenchymal progenitor cells derived from traumatized muscle tissue. J Cell Mol Med 2010 [Epub ahead of print].

57 Nesti LJ, Jackson WM, Shanti RM et al. Differentiation potential of multipotent progenitor cells derived from war-traumatized muscle tissue. J Bone Joint Surg Am 2008;90:2390–2398.

58 Amos PJ, Kapur SK, Stapor PC et al. Human adipose-derived stromal cells accelerate diabetic wound healing: Impact of cell formulation and delivery. Tissue Eng Part A 2010;16:1595–1606.

See www.StemCells.com for supporting information available online.